Journal of Biomedical Optics 9(1), 207–212 (January/February 2004)

Determination of burn depth by polarization-sensitive optical coherence tomography

Shyam M. Srinivas
Johannes F. de Boer
Hyle Park
Kourosh Keikhanzadeh
Huai-en L. Huang
Jun Zhang
Woong Qyu Jung
Zhongping Chen
J. Stuart Nelson
University of California, Irvine
Beckman Laser Institute
Department of Biomedical Engineering and Surgery
Irvine, California 92612
E-mail: snelson@laser.bli.uci.edu

Abstract. An assessment of burn depth is a key step in guiding the treatment of patients who have sustained thermal injuries. Polarization-sensitive optical coherence tomography (PS-OCT) might eventually provide the physician with a quantitative estimate of actual burn depth. Burns of various depths were induced by contacting rat skin with a brass rod preheated to 75 °C for 5, 15, or 30 s. Thermal injury denatured the collagen in the skin, and PS-OCT imaged the resulting reduction of birefringence through the depth-resolved changes in the polarization state of light propagated and reflected from the sample. Stokes vectors were calculated for each point in the PS-OCT images and the reduction in the rate of phase retardation between two orthogonal polarizations of light (deg/μm) was found to show a consistent trend with burn exposure time. PS-OCT is a noninvasive technique with potential to give the physician the information needed to formulate an optimal treatment plan for burn patients.
[DOI: 10.1117/1.1629680]

Keywords: birefringence; burn diagnosis; noninvasive imaging; optical biopsy; partial thickness burn; thermal injury.

Paper 02038 received Jun. 17, 2002; revised manuscript received Jun. 9, 2003; accepted for publication Jul. 1, 2003.

1 Introduction

Estimates related to the annual incidence of burns in the United States include 5500 deaths (1991), 51,000 acute hospital admissions (1991 to 1993 average), and 1.25 million total burn injuries (1992).[1] Traditionally, burns have been divided into first-, second-, or third-degree injuries. This classification is in many respects retrospective. A first-degree burn is limited to the epidermis and is not considered a clinical problem, since the body will regenerate damaged epithelial cells. A second-degree or partial thickness burn injures the epidermis and upper dermis; however, the skin can still heal by reepithelialization. A third-degree burn consists of full-thickness damage to the epidermis and dermis and fails to heal by regeneration of epithelium from within the wound margins.

The treatment for a full-thickness burn is skin grafting, either autologous or transplanted. However, a partial-thickness burn, which shows destruction of the epidermis and a portion of the underlying dermis, may require a more complicated treatment plan depending on the depth of dermal injury. Currently, if a patient has a suspected superficial partial thickness burn, the physician will often wait 2 to 3 weeks to determine if the wound will heal spontaneously from surviving epithelial appendages. If the burn has not healed within this time period, then the decision to graft skin is made. This necessarily prolongs treatment and puts the patient at risk of developing infection at the burn site. If a patient becomes septic with *Pseudomonas aeruginosa*, the most common opportunistic bacteria that infect burn wounds, mortality approaches 50%.[2] Conversely, if a deep partial-thickness burn is encountered, then skin grafting should be considered as soon as possible, since there is a lower incidence of infection with early eschar removal.[3] The determination of whether a partial-thickness burn is superficial or deep by visual inspection is difficult, since the distinction is based on cell viability within the dermal layers of skin.

A number of methods have been tried to determine the depth of burn injury, including the use of indocyanine green dye fluorescence,[4] vital dyes, fluorescein fluorometry, laser Doppler flowmetry (LDF), thermography, ultrasound, nuclear magnetic resonance imaging, and spectral analysis of light reflectance.[5] Most of the existing research focuses on LDF,[6–8] which is based on the fact that when burned skin sustains significant damage to dermal arterioles, capillaries, and venules, blood flow is reduced.[3] However, because of its long coherence length laser source, LDF does not provide a depth-resolved image of the blood flow in burned skin, but rather measures perfusion over the entire volume of tissue. LDF has been fraught with problems in methodology and accuracy, and as a result has been limited in its clinical use thus far.[9] Therefore, clinical observation remains the gold standard for diagnosis.[5] However, it is well known that clinical estimation of burn depth by visual and tactile assessment of the wound is highly inaccurate in determining whether a deep burn will heal, even if it is performed urgently by an experienced clinician.[3,7] A high-resolution, noncontact imaging technique is needed that would provide quantitative information on the depth of thermal damage.

Polarization-sensitive optical coherence tomography (PS-OCT) is a recently developed noninvasive optical technique that uses coherence gating to image tissue birefringence with high spatial resolution.[10] A PS-OCT image provides a two-

1083-3668/2004/$15.00 © 2004 SPIE

dimensional map of the change in the polarization state of the light with lateral and depth resolutions of 10 to 15 μm. The polarization state of light reflected from a certain depth will be changed by tissue birefringence. The total change, expressed as phase retardation between orthogonal components of the light wave, is the product of birefringence and depth. Skin has an abundance of weakly birefringent collagen molecules in the dermis. Thermal injury will denature dermal collagen, resulting in a reduction of birefringence. By comparing changes between normal and burned tissues using PS-OCT, a correlation between the depth of thermal damage and the measurable loss of skin birefringence might be established.

2 Materials and Methods

2.1 *Animal Model*

Sprague-Dawley female rats (250 to 300 g) were used as the animal model and housed in a pathogen-free facility. The animals were given a commercial base diet and water *ad libitum*. The experimental protocol was approved by the Institutional Animal Care and Use Committee at the University of California, Irvine. The rats ($n=9$) were anesthetized with an intraperitoneal injection of ketamine (87 mg/kg) and xylazine (13 mg/kg). After the animal's backs were shaved and epilated with Nair lotion hair remover (Carter-Wallace, New York, New York), experimental burns were induced in the skin following the well-established protocols of Smahel[11] and Kaufman et al.[12] A cylindrical brass rod (weight 313 g, diameter 1 cm) was preheated to 75°C in a water bath. A pair of 1-cm burns were imposed on each rat by placing the heated brass rod on contralateral portions of the animal's back for 5 ($n=3$), 15 ($n=3$), or 30 ($n=3$) s. No additional pressure was applied to the rod while it contacted the skin other than that supplied by gravity. The duration of exposure was monitored by a stopwatch.

Animals then had their burns scanned using the PS-OCT device. The measurements were all taken approximately 10 min postburn. Scans were always cross-sectional, being 4 mm long and 1 mm deep. After the scan was completed, the start and end points were marked with India ink (Higgins, Lewisburg, Tennessee) by tattooing the skin using a 30-gauge syringe needle. Selected points between the start and end points of the scan were also tattooed in the same plane. With the tattoos in place, the sites for biopsy were easily identifiable. On average, five tattoos were made for each biopsy. Tissue was taken using a 4-mm punch biopsy (Miltex, Lake Success, New York) and then processed with a regressive hematoxylin and eosin (H&E) stain for histopathological analysis. A comparable PS-OCT scan and punch biopsy were taken in a similar fashion over an area of normal skin on the back of each animal to serve as a control. The biopsy sites were sutured using 5-0 nonabsorbable nylon (Ethicon, Somerville, New Jersey). Topical antibiotic silvadene cream was then applied to the wounds, and the rat placed in a stockinette for return to the housing facility. Postoperatively, the animals were given injections of buprenorphone subcutaneously for analgesia.

2.2 *PS-OCT Device*

A schematic of the PS-OCT device is shown in Fig. 1.[13] Light from a superluminescent diode (SLD) with 0.5-mW output power, a central wavelength of 856 nm, and a spectral

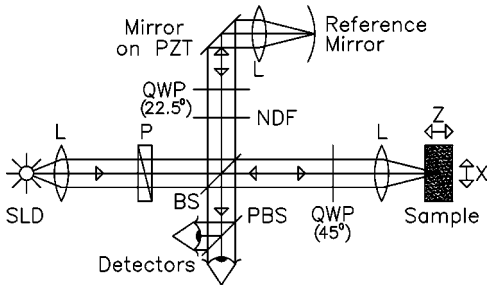

Fig. 1 Schematic of the PS-OCT device. SLD, superluminescent diode; L, lens, P, polarizer; BS, beamsplitter; QWP, quarter-wave plate; NDF, neutral-density filter; PBS, polarizing beamsplitter; PZT, piezoelectric transducer. Two-dimensional images were formed by lateral movement of the sample at constant velocity (x direction), repeated after each axial displacement (z direction).

FWHM = 25 nm was passed through a polarizer to select a pure linear horizontal input state. Light was then split into reference and sample arms by a polarization-insensitive beamsplitter. Light in the reference arm passed through a zero-order quarter-wave plate (QWP) oriented at 22.5 deg to the incident horizontal polarization. Following reflection from a mirror attached to the piezoelectric transducer (PZT), retroreflector, and return pass through the QWP, light in the reference arm had a linear polarization at 45-deg with respect to the horizontal. The mirror on the PZT modulated the reference arm length over 20 μm to generate a carrier frequency. The PZT retroreflector assembly was mounted on a translation stage to allow active focus tracking in the sample.[14] For an improved signal-to-noise ratio,[15] a neutral density filter positioned in the reference arm reduced intensity noise by a factor of 50.

Light in the sample arm passed through a QWP oriented at 45-deg to the horizontal, producing circularly polarized light incident on the tissue. After double passage through a lens ($f=50$ mm) and the tissue, and propagation through the QWP, light in the sample arm was in an arbitrary (elliptical) polarization state, determined by tissue birefringence. After recombination in the detection arm, light was split into horizontal and vertical components by a polarizing beamsplitter and focused ($f=50$ mm) on 25-μm diameter pinholes placed directly in front of the detectors to detect a single polarization and spatial mode.

Two-dimensional images were formed by lateral movement of the sample at a constant velocity of 1 mm/s (x direction), repeated after each axial displacement in depth (z direction). The carrier frequency (≈ 6 kHz) was generated by displacing the PZT-driven mirror with a 100-Hz sawtoothed wave form. Lateral and axial image resolutions were approximately 15 and 10 μm, respectively, determined by the beam waist at the focal point and the coherence length of the source. Pixel sizes in the images were 10×10 μm. The refractive index of the tissue was taken as 1.4.

The polarization state in each arm of the interferometer was computed using the Jones matrix formalism, which has been previously described in detail.[10] The horizontal and vertical polarized components of the interference intensity between light in the sample and reference arms were detected

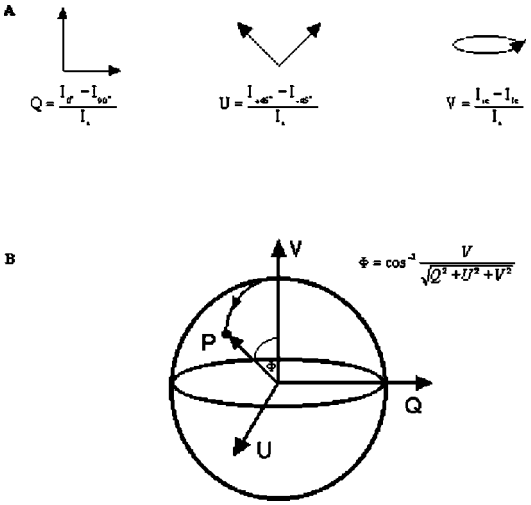

Fig. 2 Definitions of Stokes vector elements (a) and Φ parameter (b) shown with a general Stokes vector pointing to the point P on the Poincaré sphere. (a) The four Stokes parameters are denoted as I, Q, U, and V. The I_t parameter represents the total light intensity and is independent of the polarization state. Q represents the difference between the intensities of light linearly polarized at 0 deg ($I_{0°}$) and 90 deg ($I_{90°}$), normalized to the total intensity. U represents the difference in intensities of light linearly polarized at +45 deg ($I_{+45°}$) and −45 deg ($I_{-45°}$) normalized to the total intensity. V represents the difference in intensities of right (I_{rc}) and left (I_{lc}) circularly polarized light, normalized to the total intensity. (b) Φ is defined as the angle between the positive V axis and the P Stokes vector, and it measures phase retardation given a circularly polarized input state of light ($V = \pm 1$).

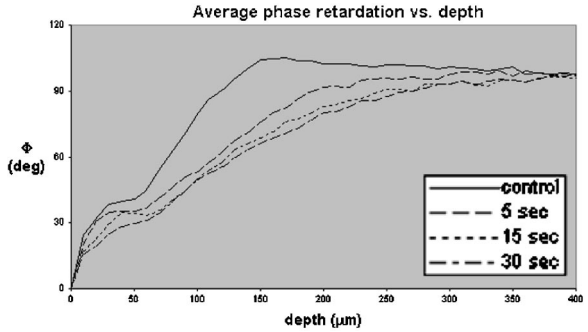

Fig. 3 Plots of average phase retardation versus depth. Φ (the phase retardation in degrees) is averaged over the entire scan length (x direction) and then plotted against depth (z direction). Φ plots were averaged according to burn exposure time: The "control" plot of Φ represents the average Φ of all the control scans ($n=9$); the "5 sec" plot represents the average Φ of all the 5-s burn scans ($n=6$); the "15 sec" plot represents the average Φ of all the 15-s burn scans ($n=6$), and the "30 sec" plot represents the average Φ of all the 30-s burn scans ($n=5$). This figure shows a clear trend between the reduction of the phase retardation versus depth, and burn severity, which could be used to obtain a burn depth estimate from the depth of histological damage that corresponds to each burn duration (Table 1).

separately. From these two quantities, the Stokes vector at each point in the scan could be calculated.[16] A Stokes vector has four parameters: one that represents the intensity of the light (I), two that represent linear polarization with reference frames separated by 45 deg (Q and U), and one that represents circular polarization (V). These four parameters uniquely represent any polarization state of light [Fig. 2(a)].

The PS-OCT images were formed by plotting and gray-scale coding V from 1 (black) to −1 (white). A white contour line corresponding to $V=0$ in the PS-OCT image was plotted and overlaid with the original image. The Φ parameter as defined by Poincaré's sphere will be a measure of the phase retardation the light experienced in the tissue [Fig. 2(b)]. Since light incident on the sample was circularly ($V=1$) polarized, $V=0$ corresponds to $\Phi=90$ deg (or 90 deg of phase retardation). Φ is a measure of phase retardation in degrees and was determined for each scan by averaging the calculated Φ values along the x direction (lateral), correcting for inadvertent skin surface inclination, and then plotting the Φ parameter (phase retardation) against depth. Figure 3 shows a plot of the average phase retardation versus depth for scans performed in this study. These Φ plots were averaged according to their burn exposure time.

2.3 *Histological Analysis*

To determine the relationship between loss of skin birefringence and actual depth of thermal damage, PS-OCT scans were compared with histological sections obtained from biopsied tissue. Inasmuch as biopsies were tattooed with India ink as previously described, the histological section corresponds to the same site optically imaged with the PS-OCT device. Since all tissue containing India ink was recovered, and the microtome used made slices in 6-μm steps, approximately 20 to 40 slices per biopsy were obtained.

Using burn parameters similar to these described by Smahel[11] on rat skin, partial- and full-thickness injuries were expected. In analyzing the histological sections, the criteria previously described by Panke and McLeod[17] were followed. Burn depth was determined by examining for the presence or absence of viable adnexal structures, such as hair follicles and sweat glands. If such structures appeared abnormal or otherwise damaged, then it can be inferred that the depth of thermal injury is at least that deep. The regressive H&E stain helped determine actual burn depth by showing a color change to dark purple for thermally denatured dermal collagen.

Also, distinct changes in dermal morphology can be observed in thermally damaged tissue. The normal dermis is made up of irregular collagen fibers and fibroblasts having an orientation roughly parallel to the skin surface. When skin is thermally damaged, the fibers lose their linearity, become fused with their neighbors, and appear as dense clumps of collagen. This hyalinization (glasslike appearance) is distinctive for thermal damage.[17,18] All these indicators were used to determine the actual depth of burn injury. The regressive H&E-stained slides were placed under an Olympus BH-2 microscope containing a reticle eyepiece. Using the ruler built into the microscope, the actual burn depth in micrometers (± 5 μm) was measured in each histological section. The burn depth reported is the average of the depths determined individually from each of the 20 to 40 histological sections. The histological analysis was done independently from the PS-OCT scan Φ determination (Table 1).

Table 1 Summary of histological data.

Duration of Exposure to Brass Rod at 75°C (s)	Average Histologically Determined Burn Depth (μm)
5	218
15	335
30	841

3 Results

Figure 4 shows *in vivo* OCT structural and phase retardation imaging of normal and burned rat skin. The probe scans across the boundary of normal and burned skin. Although we can clearly see the change in the phase retardation image between the normal and burned skin, the structural image for normal and burned skin appears very similar. Figure 3 shows a clear trend between the length of burn exposure and reduction in the slope of Φ (phase retardation versus depth). By having a trend between burn exposure time and histologically verified depth of thermal damage (Table 1), we can eventually correlate the slope of Φ to the actual burn depth. A definite trend can be seen where Φ changes at a different rate within the first few hundred micrometers, depending on burn severity. Whereas Fig. 3 summarizes the total results of our experiment, Fig. 5 shows one scan from each category as a subset of the results.

Figure 5 shows typical PS-OCT scans and the corresponding histology for normal rat skin and burns induced by contact with a preheated 75 °C brass rod for 5, 15, or 30 s, respectively. Figure 5(a1) shows a control PS-OCT image, and Fig. 5(b1) displays the abundance of intact hair follicles found in normal rat skin histology. In Fig. 5(a2) (5-s contact) the white 90-deg phase retardation line is deeper into the skin, while Fig. 5(b2) shows a corresponding purple region near the surface, indicating damage to the dermis. Figure 5(b2) would be classified as a superficial partial-thickness (second-degree) burn, being about 230 μm in depth, as indicated by the black arrows. In Fig. 5(a3) (15-s contact), the white 90-deg phase retardation line is even deeper into the skin, and the purple region indicating damage to the dermis has also increased in depth [Fig. 5(b3)]. Hair follicle damage can be seen, and Fig. 5(b3) would be classified as a deep partial-thickness (second-degree) burn, being about 400 μm in depth, as indicated by the black arrows.

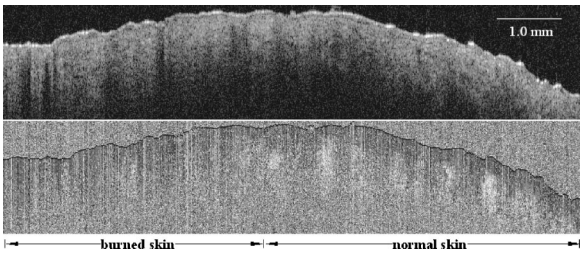

Fig. 4 PS-OCT structural (top) and phase retardation (bottom) images of normal and burned back skin of a rat. The probe scans across the boundary of normal and burned skin.

Figure 5(a4) (30-s contact) shows the deepest white 90-deg phase retardation line, while the regressive H&E stain shows damage throughout the entire dermis [Fig. 5(b4)]. Extensive hyalinization can be seen in the dermis, with damage extending to the subcutaneous fat. Figure 5(b4) would be classified as a full-thickness (third-degree) burn, being about 780 μm in depth, as indicated by the black arrows.

As can be observed in Fig. 5, PS-OCT scans of burned skin consistently show that the incident circular polarization on the samples (corresponding to 0 deg of phase retardation and coded as black) is preserved as burn depth increases. The loss of birefringence in thermally damaged tissue can clearly be seen in PS-OCT scans when they compared with normal rat skin.

4 Discussion

The loss of birefringence observed in burned skin is due to thermally induced collagen denaturation.[18] Normal collagen, a weakly birefringent material, has the ability to change the polarization state of light propagating through it. Between temperatures of 56 and 65°C, dermal collagen begins to denature[13] and the molecules become more isotropic, making skin less birefringent. The loss of birefringence in burned skin is indeed seen, as evidenced by movement of the 90-deg phase retardation line deeper into skin as the duration of exposure to thermal injury increases. As the duration and depth of thermal injury increase, there is a decrease in phase retardance per micrometer, indicating that the light is subjected to a lower rate of phase retardation, owing to the destruction of birefringent collagen molecules. Unburned control skin has the highest level of phase retardance per micrometer, as would be expected. In Figure 3, there is a significant difference in the slope of Φ when a control is compared with a 30-s exposure, and although the distinction between 5 and 15 s is small, there is a clear difference in the 90-deg phase retardation depth between the two. Once the relationship between Φ and histological burn depth has been well characterized, PS-OCT may provide quantitative information for determining burn depth.

One can observe that there is a two- to six-fold variation in the depth where $\Phi = 90$ deg in Figs. 5(a2) to 5(a4). The variation of $\Phi = 90$ deg is thought to be due to hair follicles that are abundantly present in rat skin. Hair follicles are made up of an epithelium surrounding the hair shaft. Because of their fiberlike structure, hair follicles also change the polarization state of the light. In healthy tissue, both hair follicle and collagen birefringence change the polarization state of light. As the tissue is thermally damaged, collagen birefringence decreases, but polarization changes that are due to the hair follicle structure remain. This can be seen in Figs. 5(a2) to 5(a4) in areas where the polarization still changes close to the surface. The pockets where the birefringence is clearly reduced are in the areas between the hair follicles, being primarily dermal collagen. This is clearly more pronounced in deeper burns, when the depth of the burn is as great or greater than the depth of the hair follicles.

Our justification for averaging the phase retardation over a full scan is that this will be the most rigorous method. The rate of phase retardation with thermal damage would have been even more pronounced than it is currently if we had only selected areas between the hair follicles to determine the

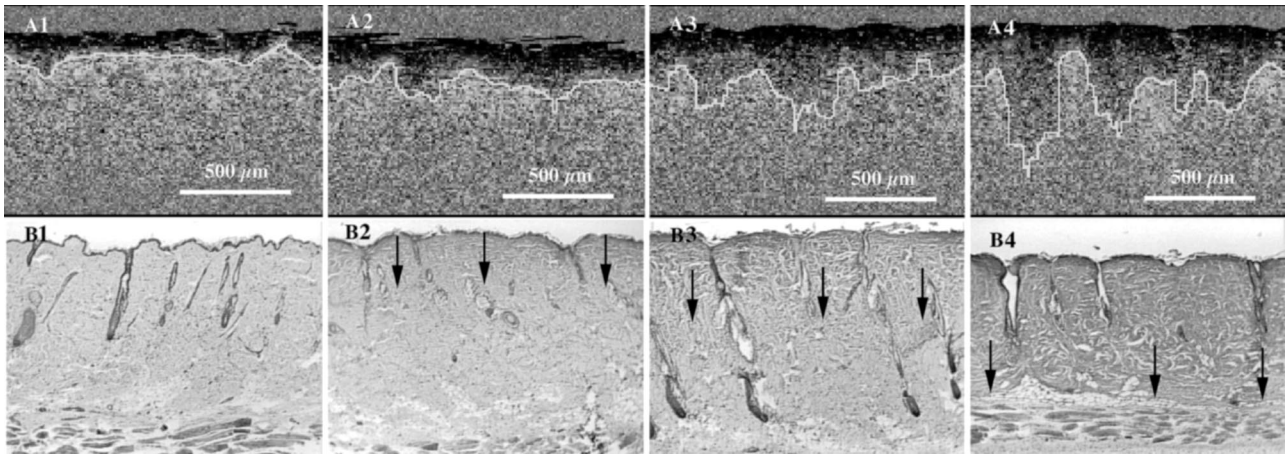

Fig. 5 Typical PS-OCT image (a) and corresponding histology (b) of normal and burned rat skin. The PS-OCT image has been gray-scale coded so that black represents 0-deg of phase retardation (the incident polarization) and white is 180-deg of phase retardation. The white contour line in the image demarcates the depth at which a 90-deg phase retardation has been reached with respect to the incident polarization. The histology and PS-OCT image has the same dimension, and the stain used for the histological image is regressive H&E. (a1) and (b1) PS-OCT image of normal skin and corresponding histology. Note the abundance of intact hair follicles. (a2) and (b2) PS-OCT of rat skin burned by contact with a 75°C brass rod for 5 s and the corresponding histology. (a3) and (b3) PS-OCT of rat skin burned by contact with a 75°C brass rod for 15 s and the corresponding histology. (a4) and (b4) PS-OCT of rat skin burned by contact with a 75°C brass rod for 5 s and the corresponding histology.

phase retardation. However, this would require us to subjectively choose hair follicle regions to exclude. Our method of taking an average over the entire scan gives the true response to thermal damage of skin that is heterogeneous in its composition.

There are two primary limitations of PS-OCT for determining burn depth. The first limitation is edema formation in response to burn injury. With increasing liquid content that is due to edema, the tissue birefringence can change as a function of time. The second limitation is the inability to detect any inflammatory response from the tissue because the method is only sensitive to structural ''form birefringence.'' Any cellular infiltrates, such as neutrophils, which begin to appear within 72 h postburn injury, cannot be detected. Bacterial invasion, a common occurrence in burn injury, will also not be detected. This is significant from a pathological point of view, since bacteria can convert partial-thickness to full-thickness burns.[19] After the first 48 h, the burn wound will begin to be infiltrated by cells, leading to granulation tissue and neovasculature, structures that are not necessarily birefringent. Thus, PS-OCT would be most useful in the initial diagnosis of burns, within the first 48 h. Also, our current PS-OCT system operates using scanning stages, which require that the sample be completely immobilized during image acquisition. Currently, each scan takes approximately 10 min. to acquire; hence the need to have the animals under general anesthesia during scanning.

Although in its current state PS-OCT is not viable for use in a clinical burn center, a new fiber-based system is under construction that will have fast scanning mirror-mounted galvanometers to allow image acquisition in less than 1 s. Resolution will be improved as well, with the use of broader bandwidth light sources with shorter coherence lengths. Our new-generation PS-OCT source will have a center wavelength of 1300 nm, which should allow a deeper penetration of up to 1 mm, bringing us into the regime of imaging human skin.

As PS-OCT evolves and the ability to scan at much faster rates is developed, this method could provide the physician with a high-resolution ''optical biopsy'' of the burn. When differentiating between superficial partial-thickness and deep partial-thickness burns, based on the depth of thermal injury, the physician may ultimately be able to make an early decision as to whether a skin graft is indicated. The noninvasive and compact nature of the PS-OCT system suggests it has the potential for use in the clinical management of burn patients and in helping the physician optimize treatment.

Acknowledgments

The authors would like to thank Leacky Liaw for her expertise in histology, Laurie Newman for her assistance with animal handling, and Christopher Saxer for his help with data presentation. This work was supported by research grants awarded by the National Institutes of Health (EB-00255, EB-00293, EB-002495, RR-01192, and AR47551). Support from the Air Force Office of Scientific Research (F49620-00-1-0371), and the Beckman Laser Institute Endowment is also gratefully acknowledged.

References

1. P. A. Brigham and E. McLoughlin, ''Burn incidence and medical care use in the United States: estimates, trends, and data sources,'' *J. Burn Care Rehabil.* **17**, 95–107 (1996).
2. K. S. Black, C. W. Hewitt, S. Smelser, et al. ''Cyclosporine and skin allografts for the treatment of thermal injury,'' *Transplantation* **45**, 13–16 (1988).
3. D. H. Park, J. W. Hwang, K. S. Jang, D. G. Han, K. Y. Ahn, and B. S. Baik, ''Use of laser Doppler flowmetry for estimation of the depth of burns,'' *Plast. Reconstr. Surg.* **101**, 1516–1523 (1998).

4. R. L. Sheridan, K. T. Schomaker, L. C. Lucchina, et al. ''Burn depth estimation by use of indocyanine green fluorescence: initial human trial,'' *J. Burn Care Rehabil.* **16**, 602–604 (1995).
5. D. Heimbach, L. Engrav, B. Grube, and J. Marvin ''Burn depth: a review,'' *World J. Surg.* **16**, 10–15 (1992).
6. Z. B. M. Niazi, T. J. H. Essex, R. Papini, D. Scott, N. R. McLean, and M. J. M. Black, ''New laser Doppler scanner, a valuable adjunct in burn depth assessment,'' *Burns* **19**, 485–489 (1993).
7. K. Waxman, N. Lefcourt, and B. Achauer, ''Heated laser Doppler flow measurements to determine depth of burn injury,'' *Am. J. Surg.* **157**, 541–543 (1989).
8. L. Atiles, W. Mileski, K. Spann, G. Purdue, J. Hunt, and C. Baxter, ''Early assessment of pediatric burn wounds by laser Doppler flowmetry,'' *J. Burn Care Rehabil.* **16**, 596–601 (1995).
9. E. K. Yeong, R. Mann, M. Goldberg, L. Engrav, and D. Heimbach, ''Improved accuracy of burn wound assessment using laser Doppler,'' *J. Trauma* **40**, 956–962 (1996).
10. J. F. de Boer, T. E. Milner, M. J. C. van Gemert, and J. S. Nelson, ''Two-dimensional birefringence imaging in biological tissue by polarization-sensitive optical coherence tomography,'' *Opt. Lett.* **22**, 934–936 (1997).
11. J. Smahel, ''Viability of skin subjected to deep partial skin thickness thermal damage: experimental studies,'' *Burns* **17**, 17–24 (1991).
12. T. Kaufman, S. N. Lusthaus, U. Sagher, and M. R. Wexler, ''Deep partial skin thickness burns: a reproducible animal model to study burn wound healing,'' *Burns* **16**, 13–16 (1990).
13. J. F. de Boer, S. M. Srinivas, A. Malekafzali, Z. Chen, and J. S. Nelson, ''Imaging thermally damaged tissue by polarization sensitive optical coherence tomography,'' *Opt. Express* **3**, 212–218 (1998).
14. Z. Chen, T. E. Milner, D. Dave, and J. S. Nelson, ''Optical Doppler tomographic imaging of fluid flow velocity in highly scattering media,'' *Opt. Lett.* **22**, 64–66 (1997).
15. W. V. Sorin and D. M. Baney, ''A simple intensity noise reduction technique for optical low-coherence reflectometry,'' *IEEE Photonics Technol. Lett.* **4**, 1404–1406 (1992).
16. J. F. de Boer, T. E. Milner, and J. S. Nelson, ''Determination of the depth-resolved Stokes parameters of light backscattered from turbid media by use of polarization-sensitive optical coherence tomography,'' *Opt. Lett.* **24**, 300–302 (1999).
17. T. W. Panke and C. G. McLeod, *Pathology of Thermal Injury: A Practical Approach*, 1st ed., pp. 23–29, Grune & Stratton, Inc., Orlando Fl (1985).
18. S. Thomsen, ''Pathologic analysis of photothermal and photomechanical effects of laser-tissue interactions,'' *Photochem. Photobiol.* **53**, 825–835 (1991).
19. P. W. Curreri, I. N. Burns, S. I. Schwartz, G. T. Shires, F. C. Spencer, and E. H. Storer, Eds., *Principles of Surgery*, 3rd ed., pp. 285-301, McGraw-Hill, Inc., New York (1979).